

# High contrast ballistic imaging using femtosecond optical Kerr gate of tellurite glass

Wenjiang Tan,<sup>1</sup> Zhiguang Zhou,<sup>2</sup> Aoxiang Lin,<sup>2</sup> Jinhai Si,<sup>1,\*</sup> Pingping Zhan,<sup>1</sup> Bin Wu,<sup>1</sup> and Xun Hou<sup>1</sup>

<sup>1</sup>Key Laboratory for Physical Electronics and Devices of the Ministry of Education, Shanxi Key Lab of Information Photonic Technique, School of Electronic and Information Engineering, Xi'an Jiaotong University, Xianning-xilu 28, Xi'an, 710049, China

<sup>2</sup>State Key Laboratory of Transient Optics and Photonics, Xi'an Institute of Optics and Precision Mechanics (XIOPM), Chinese Academy of Sciences (CAS), Xi'an 710119, China

\*[jinhaisi@mail.xjtu.edu.cn](mailto:jinhaisi@mail.xjtu.edu.cn)

**Abstract:** We investigated the ballistic imaging technique using femtosecond optical Kerr gate of a tellurite glass. High contrast images of an object hidden behind turbid media were obtained. Compared to the conventional femtosecond optical Kerr gate using fused quartz, the optical Kerr gate using tellurite glass has more capacity to acquire high quality images of the object hidden behind a high optical density turbid medium. The experimental results indicated that the tellurite glass is a good candidate as the optical Kerr material for the ballistic imaging technique due to its large optical nonlinearity.

©2013 Optical Society of America

**OCIS codes:** (190.3270) Kerr effect; (190.4400) Nonlinear optics, materials; (290.7050) Turbid media; (290.4210) Multiple scattering.

---

## References and links

1. M. Paciaroni and M. A. Linne, "Single-shot, two-dimensional ballistic imaging through scattering media," *Appl. Opt.* **43**(26), 5100–5109 (2004).
2. M. E. Zevallos L, S. K. Gayen, M. Alrubaiee, and R. R. Alfano, "Time-gated backscattered ballistic light imaging of objects in turbid water," *Appl. Phys. Lett.* **86**(1), 011115 (2005).
3. L. Wang, P. P. Ho, C. Liu, G. Zhang, and R. R. Alfano, "Ballistic 2-d imaging through scattering walls using an ultrafast optical Kerr gate," *Science* **253**(5021), 769–771 (1991).
4. J. Tong, Y. Yang, J. Si, W. Tan, F. Chen, W. Yi, and X. Hou, "Measurements of the scattering coefficients of intralipid solutions by a femtosecond optical Kerr gate," *Opt. Eng.* **50**(4), 043607 (2011).
5. D. J. Hall, J. C. Hebden, and D. T. Delpy, "Imaging very-low-contrast objects in breastlike scattering media with a time-resolved method," *Appl. Opt.* **36**(28), 7270–7276 (1997).
6. J. Selb, D. K. Joseph, and D. A. Boas, "Time-gated optical system for depth-resolved functional brain imaging," *J. Biomed. Opt.* **11**(4), 044008 (2006).
7. M. Paciaroni, M. A. Linne, T. Hall, J. P. Delplanque, and T. Parker, "Single-shot two-dimensional ballistic imaging of the liquid core in an atomizing spray," *Atom. Sprays* **16**(1), 51–70 (2006).
8. M. A. Linne, M. Paciaroni, J. R. Gord, and T. R. Meyer, "Ballistic imaging of the liquid core for a steady jet in crossflow," *Appl. Opt.* **44**(31), 6627–6634 (2005).
9. J. B. Schmidt, Z. D. Schaefer, T. R. Meyer, S. Roy, S. A. Danczyk, and J. R. Gord, "Ultrafast time-gated ballistic-photon imaging and shadowgraphy in optically dense rocket sprays," *Appl. Opt.* **48**(4), B137–B144 (2009).
10. M. A. Linne, D. Sedarsky, T. R. Meyer, J. R. Gord, and C. Carter, "Ballistic imaging in the near-field of an effervescent spray," *Exp. Fluids* **49**(4), 911–923 (2010).
11. C. Dunsby and P. M. W. French, "Techniques for depth-resolved imaging through turbid media including coherence-gated imaging," *J. Phys. D Appl. Phys.* **36**(14), R207–R227 (2003).
12. S. Idlahcen, L. Méès, C. Rozé, T. Girasole, and J. B. Blaisot, "Time gate, optical layout, and wavelength effects on ballistic imaging," *J. Opt. Soc. Am. A* **26**(9), 1995–2004 (2009).
13. A. Kuditcher, B. G. Hoover, M. P. Hehlen, E. N. Leith, S. C. Rand, and M. P. Shih, "Ultrafast, cross-correlated harmonic imaging through scattering media," *Appl. Opt.* **40**(1), 45–51 (2001).
14. A. Bassi, D. Brida, C. D'Andrea, G. Valentini, R. Cubeddu, S. De Silvestri, and G. Cerullo, "Time-gated optical projection tomography," *Opt. Lett.* **35**(16), 2732–2734 (2010).
15. A. Mermillod-Blondin, C. Maclair, J. Bonse, R. Stoian, E. Audouard, A. Rosenfeld, and I. V. Hertel, "Time-resolved imaging of laser-induced refractive index changes in transparent media," *Rev. Sci. Instrum.* **82**(3), 033703 (2011).

16. J. Tong, W. Tan, J. Si, F. Cheng, W. Yi, and X. Hou, "High time-resolved imaging of targets in turbid media using ultrafast optical Kerr gate," *Chin. Phys. Lett.* **29**(2), 0242072–1-3 (2012).
17. D. R. Symes, U. Wegner, H.-C. Ahlswede, M. J. V. Streeter, P. L. Gallegos, E. J. Divall, R. A. Smith, P. P. Rajeev, and D. Neely, "Ultrafast gated imaging of laser produced plasmas using the optical Kerr effect," *Appl. Phys. Lett.* **96**(1), 011109 (2010).
18. F. X. d'Abzac, M. Kervella, L. Hespel, and T. Dartigalongue, "Experimental and numerical analysis of ballistic and scattered light using femtosecond optical Kerr gating: a way for the characterization of strongly scattering media," *Opt. Express* **20**(9), 9604–9615 (2012).
19. J. Tong, W. Tan, J. Si, W. Cui, W. Yi, F. Chen, and X. Hou, "Femtosecond optical Kerr effect measurement using supercontinuum for eliminating the nonlinear coherent coupling effect," *J. Opt.* **14**(4), 045203 (2012).
20. A. J. Taylor, G. Rodriguez, and T. S. Clement, "Determination of  $n_2$  by direct measurement of the optical phase," *Opt. Lett.* **21**(22), 1812–1814 (1996).
21. R. F. Souza, M. A. R. C. Alencar, J. M. Hichmann, R. Kobayashi, and L. R. P. Kassab, "Femtosecond nonlinear optical properties of tellurite glasses," *Appl. Phys. Lett.* **89**(17), 171917 (2006).
22. A. Lin, A. Zhang, E. J. Bushong, and J. Toulouse, "Solid-core tellurite glass fiber for infrared and nonlinear applications," *Opt. Express* **17**(19), 16716–16721 (2009).
23. S. J. Madden and K. T. Vu, "Very low loss reactively ion etched Tellurium Dioxide planar rib waveguides for linear and non-linear optics," *Opt. Express* **17**(20), 17645–17651 (2009).
24. W. Tan, Z. Zhou, A. Lin, J. Si, J. Tong, and X. Hou, "Femtosecond nonlinear optical property of a TeO<sub>2</sub>-ZnO-Na<sub>2</sub>O glass and its application in time-resolved three-dimensional imaging," *Opt. Commun.* **291**, 337–340 (2013).
25. L. Wang, P. P. Ho, X. Liang, H. Dai, and R. R. Alfano, "Kerr - Fourier imaging of hidden objects in thick turbid media," *Opt. Lett.* **18**(3), 241–243 (1993).

---

## 1. Introduction

Time-gated ballistic-photon imaging (commonly referred to as ballistic imaging) is a kind of special optical shadowgraph imaging that employs a short time gate to suppress multiply scattered photons and improve the visualization of objects hidden in the turbid media [1,2]. It relies on the fact that ballistic photons propagating straight through a turbid media without scattering will exit earlier than the multiply scattered photons [3,4]. This optical diagnosis technique is originally developed for medical applications [5,6], for instance, to detect human tumors in soft tissue. Recently, ballistic imaging technique has been implemented to investigate the dynamics of high-pressure diesel sprays and liquid jets in gaseous cross-flow [7–9]. Because it has the ability to acquire breakup information from dense region of the spray that is heretofore inaccessible to conventional imaging technique [10].

A number of nonlinear optical phenomena [11], for example the optical Kerr effect [12] and the second harmonic generation [13], have been demonstrated to have the potential for the application of the ballistic imaging. However, most ballistic imaging systems have gradually taken the advantage of the optical Kerr gate (OKG) to mitigate scattered photons due to its advantages, such as no need of satisfaction of the phase-matching condition or high intensity of the imaging signal [14–17]. An amplified femtosecond laser is often used as the ideal light source to activate the OKG for photon discrimination. It is especially important when the approximate time spread of ballistic versus multiply scattered photons is of the order of several picoseconds [9,18].

As the key factor of the performance of the OKG, a suitable Kerr material should be of large nonlinearity, ultrafast response time, and wide transparent window, which could offer higher signal-to-noise ratio, better temporal resolution, and wider applicable wavelength range. However, there is an inherent tradeoff between high sensitivity and fast response in the applications based on the OKG in femtosecond regime. For example, as two widely used optical Kerr materials, carbon disulfide owns very large optical nonlinearity but suffers a slow relaxation time of about 1.6 ps [19], and the fused quartz has ultrafast response but suffers a low optical nonlinearity of about  $2.48 \times 10^{-16}$  cm<sup>2</sup>/W [20]. Recently, it has emerged that the tellurite glass seems to be a preferable nonlinear optical material because of its large optical nonlinearity, ultrafast response time, low phonon energy, and good thermal and mechanical stability, which has been extensively exploited in many nonlinear optical applications [21–24].

In this study, we investigated the ballistic imaging technique using femtosecond OKG of a tellurite glass. High contrast images of a 1.41-line-pair/mm (1.41-lp/mm) section of the

resolution test chart hidden behind turbid media were obtained. Compared to the conventional femtosecond OKG using fused quartz, the OKG using tellurite glass has more capacity to acquire high quality images of the object hidden behind the high optical density turbid media due to its large optical nonlinearity.

## 2. Experiments

Figure 1 shows the schematic of the ballistic imaging system in our measurement. A Ti:sapphire laser system, emitting 50 fs, 4 mJ, and 800 nm laser pulses at a repetition rate of 1 kHz, was used in our experiments. The laser beam was split into two parts by using a short pass filter (SPF). Two neutral attenuators ( $NA_1$  and  $NA_2$ ) were used to adjust their intensities. The reflective part, passing through an optical delay translation and a half-wave plate ( $\lambda/2$ ), was focused onto an optical Kerr material as the gating beam by a lens ( $L_1$ ). The half-wave plate was used to control its polarization for the maximum gating efficiency. The transmitted part was modulated by a 1.41- $\mu\text{m}$  section of the resolution test pattern (a United States Air Force test pattern) and passed through turbid media as the imaging beam. The turbid media used here were various concentrations of suspensions of 0.4- $\mu\text{m}$ -diameter polystyrene microspheres filled in a 10 mm path-length sample cell. In our experiments, the energy of the gating beam was about 18  $\mu\text{J}/\text{pulse}$ , while the energy of the imaging beam was about 288  $\mu\text{J}/\text{pulse}$ . The spot diameters at the optical Kerr material surface of the gating beam and the imaging beam were measured to be about 120  $\mu\text{m}$  and 100  $\mu\text{m}$ , respectively.

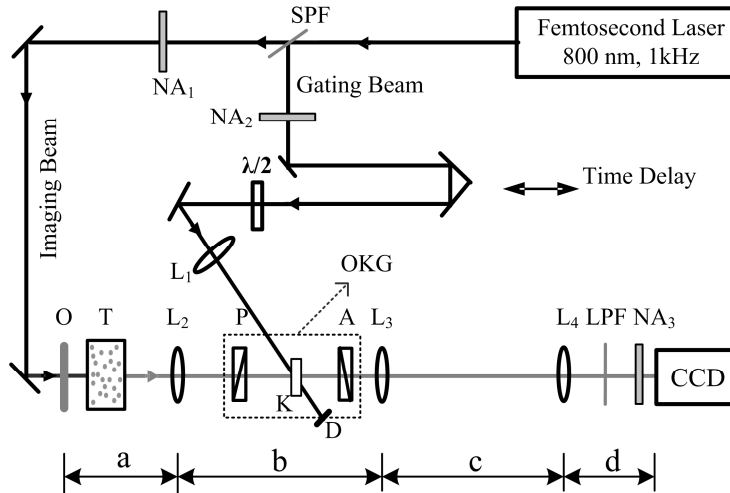


Fig. 1. Schematic of the ballistic imaging system in our experiment. SPF, short pass filter;  $NA_1$ ,  $NA_2$ , and  $NA_3$ , neutral attenuators;  $\lambda/2$ , half-wave plate; O, object; T, turbid media; P, polarizer; K, optical Kerr material; A, analyzer; OKG, optical Kerr gate; D, dump; LPF, long pass filter;  $L_1$ ,  $L_2$ ,  $L_3$ , and  $L_4$ , lenses with focal lengths of 180, 150, 100, and 100 mm, respectively. All the diameters of the lenses is 50 mm.  $a = 190$  mm,  $b = 250$  mm,  $c = 330$  mm,  $d = 160$  mm.

Emerging from the turbid media, the disturbed imaging beam was then collected and introduced into an OKG by a lens ( $L_2$ ). The OKG consisted of a pair of crossed polarizers (P and A) and a Kerr material between them. When the OKG was opened by the gating beam, a time-sliced imaging beam (the part of the imaging beam gated by the OKG) could pass through the analyzer. By adjusting the time delay between the gating pulse and the imaging pulse, the ballistic component of imaging beam could be temporally picked out by the OKG. After recollimation by a lens ( $L_3$ ), the imaging beam was detected by CCD camera through an imaging lens ( $L_4$ ). A long pass filter (LPF) was placed before the CCD camera to block noise light caused by the gating beam because some gating light was scattered forward into

the imaging system. A neutral attenuator ( $NA_3$ ) was used to avoid laser damage on the CCD camera, when the intensity of the gated imaging beam was too strong.

A piece of 1 mm tellurite glass with composition of  $TeO_2$ - $ZnO$ - $Na_2O$  was used here as the optical Kerr material. The nonlinear refractive index  $n_2$  of the tellurite glass was estimated to be about  $4.56 \times 10^{-15} \text{ cm}^2/\text{W}$  and the details about its preparation were given in the reference [24]. Moreover, a fused quartz plate with the same thickness was also used as the optical Kerr material for comparison. The time-resolved OKG signals of the tellurite glass and the fused quartz were measured and shown in Fig. 2. The full width at half maximum of the signals was about 200 fs. There is a little degradation of the temporal resolution because the duration of the laser pulses was expanded due to the dispersion of the optical elements. The measured spectra of the gating beam and the imaging beam were also shown in the inset of Fig. 2. Both the short and long-wave pass filters have low out-of-band transmittance less than 0.1%. The average transmittance is 80% for the long pass filter and 65% for the short pass filter.

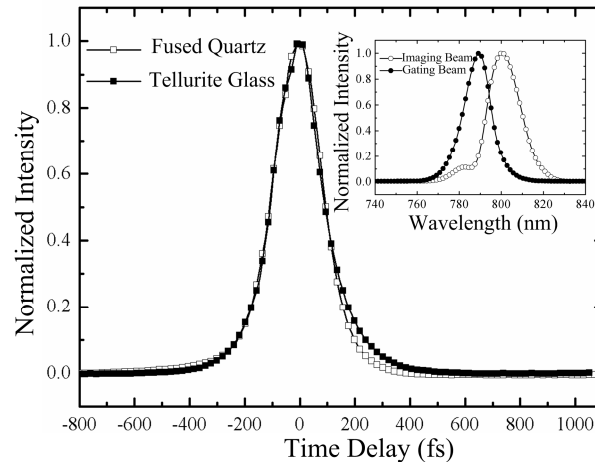


Fig. 2. The time-resolved OKG signals of the tellurite glass and the fused quartz. The inset shows the spectra of the gating and imaging beams.

### 3. Results and discussion

The 1.41-1p/mm section of the resolution test pattern was selected as the imaging object. Firstly, we filled the sample cell with the distilled water and obtained the image of the object without using the OKG as shown in Fig. 3(a). Then, we filled the sample cell with the dense suspensions of 0.4- $\mu\text{m}$ -diameter polystyrene microspheres and obtained a seriously disturbed image of the object as shown in Fig. 3(b). Finally, we acquired the image of the object using the OKG with the same turbid media as shown in Fig. 3(c). We can see that the ballistic imaging greatly improved the visualization of the object and almost retains its undistorted structure information. It should be noted that the boundary sharpness of the ballistic images decreased to a certain extent due to the low-pass spatial filtering effect of the OKG [25].

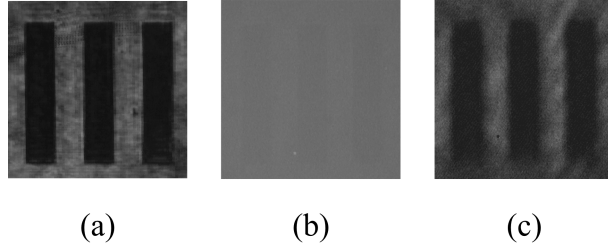


Fig. 3. Images of a 1.41-1p/mm section of the resolution test pattern from the ballistic imaging system in our experiment. (a) sample cell filled with distilled water without using the OKG. (b) sample cell filled with dense suspensions of polystyrene microspheres without using the OKG. (c) sample cell filled with dense suspensions of polystyrene microspheres using the OKG.

To further analysis the performance of the ballistic imaging at different optical densities of the turbid media, we then varied the concentrations of the suspensions of polystyrene microspheres and obtained some ballistic images at different optical densities of 7.4, 8.0, 8.7, 9.3, 9.8, 10.2 and 11.5 using the OKG of the tellurite glass. The disturbed images without using the OKG were also taken for comparison. We calculated the contrast of all the images as:

$$Contrast = \frac{I_{\max} - I_{\min}}{I_{\max} + I_{\min}} \quad (1)$$

Where  $I_{\max}$  is the average image intensity of the unshadowed parts in the square-wave grating region and  $I_{\min}$  is the average image intensity of the shadowed parts in the square-wave grating region of the object.

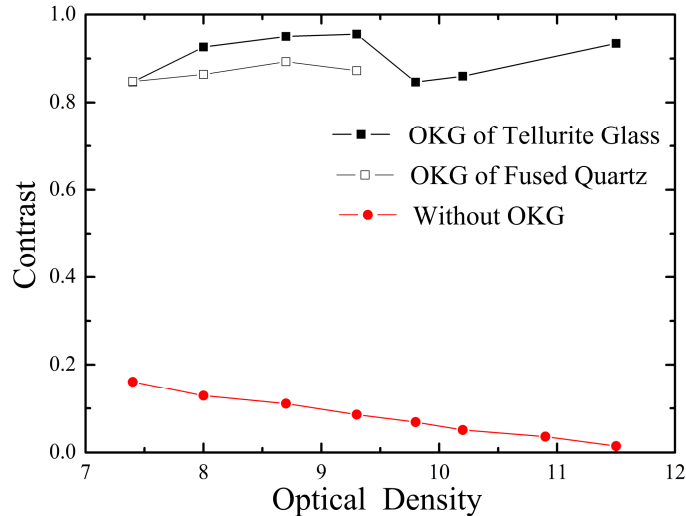


Fig. 4. Imaging contrasts with and without using the OKG at different optical densities of the turbid media.

From Fig. 4, we can see that the image contrasts using the OKG vary from 0.85 to 0.92. The contrasts of the images without using the OKG decrease from 0.18 to 0.01 with the increasing of the optical densities of the turbid media. The ballistic imaging contrast is improved by more than 67% compared with the direct imaging. At the same optical density, the contrast for the ballistic imaging is much higher than that for the directly imaging because the OKG can effectively eliminate the scattered photons which obviously deteriorate

the image contrast. These results indicated that ballistic imaging using the OKG was an effective method to improve the visualization of objects hidden in the turbid media.

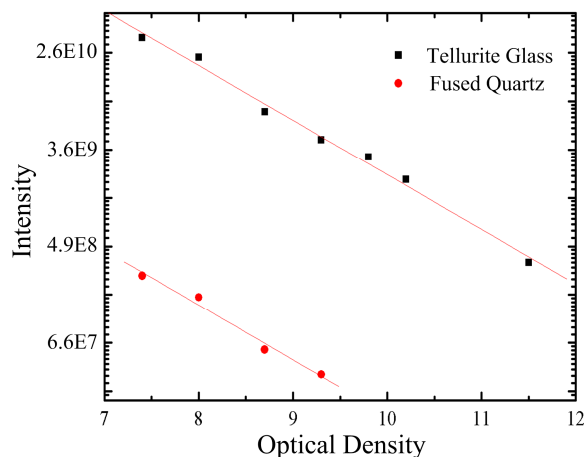


Fig. 5. Ballistic-imaging intensities versus optical densities for the tellurite glass and the fused quartz.

Furthermore, we compared the performance of the ballistic imaging using the OKG of the tellurite glass, or using the OKG of the fused quartz. Figure 5 shows the ballistic-imaging intensities for these two materials. Plotted on the nature logarithmic ordinate is the relative intensity of these images versus the optical density of the turbid media. In our experiment, the transmittance of the OKG using the tellurite glass is about 21% but only about 0.13% for the fused quartz in the same condition due to their distinctly different optical nonlinearities. So we can see that the ballistic-imaging intensity for the tellurite glass is much larger than that for the fused quartz at the same optical density from Fig. 5. And the ballistic-imaging intensity decreased with increasing the optical density of the turbid media. As a result, the optical Kerr gated imaging beam would be unable to form an image, when its intensity was not high enough to reach the sensitivity limitation of the CCD camera used here. The maximum measurable optical density for the tellurite glass in our experiment is measured to be about 11.5 but only about 9.3 for the fused quartz as shown in Fig. 5. These results indicated that ballistic imaging using the OKG of the tellurite glass could be more suitable for dense turbid media. From Fig. 5, we can also see that there is a good linear relationship between the logarithm of the ballistic-imaging intensity and the optical density. As well known, the intensity of the pure ballistic light is attenuated in turbid media according to the Beer-Lambert relation. So this result also demonstrated that the OKG could reject the scattered photons effectively.

In addition, we also compared the ballistic-imaging contrasts versus optical densities for the tellurite glass and the fused quartz as mentioned above. From Fig. 6, we can see the ballistic-imaging contrasts for both of the optical Kerr materials are higher than 0.85 and larger than the directly-imaging contrasts obtained in Fig. 4. Besides, the imaging contrasts for the tellurite glass are slightly higher than that for the fused quartz. We inferred that the optical Kerr gated slightly-scattered photons and nonuniformities in the laser beam affect the ballistic-imaging contrast for fused quartz due to its low signal intensity. So we further compared the spatial intensity distributions of the square-wave grating region of the ballistic images for both optical Kerr materials. The inset of Fig. 6 shows a typical result at the optical density 8.7. We can see that both of the images have some intensity glitches due to the uniform laser intensity distribution and the noise light. But the images for fused quartz have more serious and comparable intensity glitches in both unshadowed and shadowed regions, which reduce the imaging contrast. While the images for the tellurite glass have negligible intensity glitches in the shadowed regions than that in the unshadowed regions because of the

large signal intensity. These results indicated that the ballistic imaging using the OKG of the tellurite glass had superiority compared to that using the OKG of the fused quartz. Moreover, there were always some slightly-scattered photons which were able to pass through the OKG. These slightly-scattered photons increased as a proportion of the optical Kerr gated photons with increasing the optical density of the turbid media. However, the amount of these slightly-scattered photons decreased gradually and was not high enough to reach the sensitivity limitation of the CCD camera with the optical density from 10 to 12 in our experiment. On the contrary, the gated ballistic photons can be still detected normally. So we can see the imaging contrast for tellurite glass in Fig. 6 increases slightly with the optical density from 10 to 12.

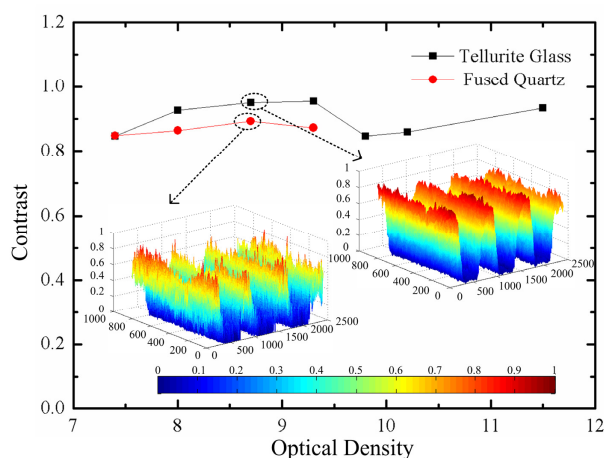


Fig. 6. Ballistic-imaging contrasts versus optical densities for the tellurite glass and the fused quartz. The inset shows the spatial intensity distributions of the ballistic images for both optical Kerr materials at the optical density 8.7.

It is worth mentioning that the transmission of the OKG equals to the product of the linear and nonlinear transmission. From the visible to the near-infrared wavelength region, the linear transmission of the tellurite glass keeps about 80% of that of the fused quartz. The transmittance of the OKG using the tellurite glass is about 21% but only about 0.13% for the fused quartz in our experiment. So we estimated the nonlinear transmission of the tellurite glass was about 130 times higher than that of the fused quartz in our experiment. In addition, the nonlinear transmission of the OKG is proportional to the square of the pump power, and not related to the probe power. It seems that the transmission of the OKG for the fused quartz could increase as high as that for the tellurite glass by increasing the pump power. However, the maximum transmittance of the fused quartz can only reach about 0.2% in our experiment to avoid the laser damage. Furthermore, the transmission of the OKG for the tellurite glass could also be higher than that for the fused quartz for the near-ultraviolet probe beam, which is just partly absorbed by the tellurite glass. So the performance of the OKG for the tellurite glass can be better than that for the fused quartz in a large spectral band.

#### 4. Conclusion

In summary, we investigated the ballistic imaging technique using the femtosecond OKG of a tellurite glass. High contrast images of a 1.41-lp/mm section of the resolution test pattern hidden behind the dense suspensions of polystyrene microspheres have been obtained. Experimental results showed that the ballistic imaging could greatly improve the visualization of object and almost retains its undistorted structure information. The image contrast is improved by more than 67% compared with the direct imaging. Compared to the conventional femtosecond OKG using the fused quartz, the maximum measurable optical density using the femtosecond OKG of the tellurite glass in our experiment is about 11.5 and

larger than that about 9.3 for the fused quartz. In addition, the ballistic images acquired with using the OKG of the tellurite glass could have larger intensity and higher contrast than that for the fused quartz. These results indicated that the tellurite glass was a good candidate as the optical Kerr material for the ballistic imaging due to its large optical nonlinearity.

#### **Acknowledgments**

The authors gratefully acknowledge the financial support for this work provided by the National Science Foundation of China under the Grant Nos. 61205129, 61235003, and 60907039, the Natural Science Basic Research Plan in Shaanxi Province of China (Program No. 2012JQ8002), and the “Hundreds of Talents Programs” from the Chinese Academy of Sciences.